Solar Physics (2023) 298:46
https://doi.org/10.1007/s11207-023-02139-0

RESEARCH

Daytime Sky Quality at El Leoncito, Argentina

F.A. Iglesias[1] · C. Francile[2] · J. Lazarte-Gelmetti[2] · L.A. Balmaceda[3,4] · H. Cremades[1] · F. Cisterna[1]

Received: 21 January 2023 / Accepted: 3 March 2023

Abstract

We characterize the daytime sky quality in terms of brightness, cloud coverage, and main weather variables at the Carlos Ulrico Cesco station of the Felix Aguilar Astronomical Observatory (OAFA), located in El Leoncito National Park, San Juan, Argentina. We have collected more than 15 years of daily observations from the auxiliary sky brightness detectors of the Mirror Coronagraph for Argentina (MICA, in operations from 1997 to 2012), including daily observing reports. We additionally present data from two meteorological stations operated at the site from 2000 to 2020. We determine the main statistical properties and seasonal variability of daytime sky brightness, clear sky time fraction (CSTF), precipitable water vapor (WV), temperature, humidity, and wind speed, which are relevant for solar, particularly coronal observations.

Our results confirm that El Leoncito is an excellent place to perform daytime astronomical observations. We measure a median sky brightness of 15.8 ppm, estimated at 526.0 ± 1.0 nm and 6 solar radii from the solar disk center; a median CSTF of 0.7; and a median WV below 6 mm. These values, and those of other relevant weather variables, are comparable to the levels found among the best astronomical observing sites in the world. Due to the extended period of time analyzed and high sampling frequency, the novel data and results presented in this report contribute to the analysis and interpretation of historical sky brightness data and are of great value for the future planning of daytime astronomical instrumentation at El Leoncito.

Keywords Earth's atmosphere: atmospheric extinction · Site testing · Corona

1. Introduction

Along with astronomical seeing, sky brightness and clear sky time fraction (CSTF) are two key factors determining site selection for conducting state-of-the-art solar observations. Modern optical solar facilities can reduce the effects of seeing by employing single and multi-conjugate adaptive optics (e.g., Schmidt et al., 2021) in combination with numeric image restoration (e.g., Suzuki et al., 2018), to reach the diffraction limit of large-aperture telescopes on the ground for a considerable portion of the observing time, provided a minimum seeing condition is given. This capability is necessary to perform high-spatial-resolution observations of the solar surface and its atmosphere. On the other hand, it is particularly challenging to overcome the undesired effects of low sky transmission and high brightness,

Extended author information available on the last page of the article

which include the reduction of signal-to-noise ratio (SNR) and contrast, particularly when imaging the extremely dim solar corona.

CSTF denotes the portion of the daytime when the sky is free of clouds or other absorbers that reduce transmission. In the optical spectral regime, atmospheric attenuation is dominated by molecular absorption due to ozone and water, Rayleigh scattering by air molecules and Mie scattering by aerosols (dust, artificial pollutants, etc.) At infrared (IR) and near IR wavelengths, e.g., near the strong atmospheric absorption band at 940 nm, the most important absorbers are H_2O, CO_2, and O_3 molecules, and aerosols (Eldridge, 1967). Thus, water vapor (WV) dominates absorption, and the best astronomical skies are found mostly at dry and high-altitude sites, e.g., Giovanelli et al. (2001).

On the other hand, sky brightness refers to the light intensity integrated over an annular portion of the sky around the solar disk and a specific wavelength range. It can be measured using Lyot coronographs (Lyot and Marshall, 1933) and is reported normalized to the solar disk brightness ($I_\odot$). Sky brightness is modulated by atmospheric scattering, particularly by air molecules and aerosols. Given that sensitive Lyot coronagraphs can be expensive and their calibration difficult, Evans (1948) developed a compact sky photometer that detects the brightness of both the solar disk and its surrounding sky simultaneously, allowing for easier normalization. The Evans photometer has been successfully employed for long-term surveys at various worldwide solar observatories, e.g., Sakurai (2002) found a mean sky brightness of 40 ppm at Norikura, Japan, in the period from 1951 to 1997. However, this instrument requires manual operation and is unpractical for higher-cadence, continuous monitoring. This is why the site survey team of the largest solar observatory, the recently commissioned 4-m Daniel K. Inouye Solar Telescope (DKIST, Rimmele et al., 2020), developed the Sky Brightness Monitor (SBM, Lin and Penn, 2004). This instrument presents a compact optical configuration with low-maintenance, where the external occulter is replaced by an ND4 filter to simultaneously measure $I_\odot$ and simplify normalization. SBM measures sky brightness using a 2D image sensor at the $10^{-6}\, I_\odot$ (1 ppm) level, within a field of view (FOV) of 4 to 8 solar radii ($R_\odot$), and at four continuum spectral bands centered at 450, 530, 890, and 940 nm.

Sky brightness is particularly critical for observations of the dim solar corona, including the estimation of its weak magnetic fields using polarimetric and/or Doppler seismology methods, which are critical to understanding wave propagation, heating, and eruptive phenomena in the corona, e.g., Judge et al. (2001). Coronal intensity is extremely low compared to the solar disk and decreases exponentially with the radial distance from the solar surface (Baumbach, 1937). The relative intensity of the white-light corona reduces approximately from 10^{-5} to 10^{-8} in the $1 - 2\, R_\odot$ range. As a reference, the sky brightness of a perfectly clear day and during a total solar eclipse are of order 10^{-6} and 10^{-8}, respectively, e.g., van de Hulst (1953). Consequently, sky brightness and CSTF are two very relevant variables to determine the best location to deploy new solar observatories. This is clearly reflected in the list of critical requirements included in notable past site selection surveys, e.g., the broad survey ended in 1991 for the GONG[1] network (Hill et al., 1994a,b).

Some of the most comprehensive and modern daytime astronomical site surveys have been done in the last two decades, or are currently undergoing, to allocate the next generation of large-aperture solar observatories. For example, the site survey working group of DKIST studied daytime seeing, sky brightness, CSTF, dust levels, and WV content in the best 6 sites of a list of 72 initial candidates[2] (Penn et al., 2004; Hill et al., 2006). Among

[1]The Global Oscillation Network Group (GONG), see Leibacher (1999).

[2]The final site survey report is available at dkist.nso.edu/site/finalreport.

Table 1 Selected DKIST site survey results (Hill et al., 2006) at three different observatories (see columns titles) obtained in the 2002 – 2004 period. We show the median sky brightness observed during ≈ 200 days (≈ 60 000 measurements) at three continuum spectral bands and 6 $R_\odot$.

Parameter	Big Bear	Haleakalā[a]	Roque de los Muchachos
Sky brightness at 890 nm [ppm]	20	1.1	5.4
Sky brightness at 530 nm [ppm]	21	2.4	11
Sky brightness at 450 nm [ppm]	19	3.1	14
Clear sky time fraction	0.712	0.619	0.639
Median wind speed [$m\,s^{-1}$]	4.7	4.5	3.6
Median temperature [°C]	16.7	13.9	10.6
Particles >0.5 μm [particles m^{-3}]	1 8298 8982	184 8661	382 8988
Particles >5 μm [particles m^{-3}]	8 8263	1 8589	2 860

[a]Similar values are found at Mauna Loa Observatory, see the end of Section 1.

these, the top candidates in terms of observing conditions were found to be the Big Bear Solar Observatory in California, Haleakalā Observatories in Hawaii, and the Observatorio Roque de los Muchachos in La Palma. After a ∼2 year survey employing SBM and other instruments, the site survey team selected the Haleakalā observatory to build DKIST. The decision was based, among other considerations, on the measured values of sky brightness and main weather parameters summarized in Table 1. We note that the excellent daytime observing conditions found by the DKIST team at these sites are a more detailed and accurate confirmation of the results found by other past site surveys, and of the high-quality data gathered during several decades by various solar observatories located there, e.g., the Swedish Solar Telescope (Rouppe van der Voort et al., 2017) or the Mauna Loa K-Coronagraph (see below). Based on such historical record, e.g., the 5-year long survey performed by the Large Earth-based Solar Telescope project (Engvold, 1991) and more recent measurements, the site selection team of the European Solar Telescope selected in 2019 the Roque de los Muchachos Observatory to allocate the upcoming 4-m class observatory (Quintero Noda et al., 2022). In addition, the SBM has been employed, with minor modifications, during the site surveys performed in preparation for the next generation of solar observatories in China (Fang, 2011). Liu et al. (2012) used the SBM to detect a sky brightness of ∼ 5 ppm and changes as small as 0.24 ppm/s at 450 nm and $4.8 - 6.1\,R_\odot$ during the annular solar eclipse of 2010 near the Cibi Lake in Yunnan, China. In addition, Zhao et al. (2014) applied segmentation algorithms to process the SBM images and automatically normalize the sky brightness to $I_\odot$. Using such a technique at the Lijiang observatory in the Yunnan province during 2011, they found that sky brightness remains under 20 ppm per unit airmass for ≈ 40% of the total observing time in a clear day (Zhao et al., 2018).

As mentioned above, coronal magnetometry requires very low sky-brightness levels. Among the most sensitive ($\sim 5\,G$) measurements of the magnetic field present in the low ($\sim 1.03 - 1.5\,R_\odot$) solar corona have been obtained in the last decade by the Coronal Multichannel Polarimeter (CoMP, Tomczyk et al., 2008), e.g., Tomczyk et al. (2007), Yang et al. (2020), from the Sunspot Solar Observatory (SSO) and Mauna Loa Observatory in Hawaii. CoMP's success motivated the development of an upgraded version (uCoMP, Landi, Habbal, and Tomczyk, 2016) located at Mauna Loa. In addition, it influenced the specification and development of the future Coronal Solar Magnetism Observatory (COSMO, Tomczyk

et al., 2016). COSMO[3] includes a 1.5-m refractive coronograph and aims at even more sensitive coronal magnetometry. COSMO optimal site requirements (Oakley, 2015) include periods of sky brightness below 2 ppm at 1074 nm, temperature of 20° C and winds below 10 m s^{-1}. Both SSO and Mauna Loa present good coronal sky conditions, similar to the sites included in Table 1. At SSO, the median sky brightness can be as low as $\sim$ 5 ppm at 890 nm, as measured with SBM (Penn et al., 2004). At Mauna Loa, where the notable Mauna Loa K-Coronagraph has provided quality images of the K-corona since 1980,[4] median sky brightness can reach $\sim$ 1.2 ppm at 890 nm also measured with SBM (Garcia and Yasukawa, 1983; Steven Tomczyk and Nelson, 2015). Liberatore et al. (2022) recently measured a sky brightness as low as 0.7 ppm at 591.25 nm and 2.24 $R_{\odot}$, at Concordia station in Antarctica, using a 5-cm internally-occulted, Lyot coronograph known as the Antarctica Solar Coronagraph.

In this paper, we report the daytime observing conditions, including sky brightness and CSTF, at the Carlos Ulrico Cesco station of the Observatorio Astronómico Félix Aguilar (OAFA[5]) located in San Juan, Argentina, using more than 15 years of observations. The rest of the paper is organized as follows: Section 2 presents the observatories at El Leoncito and the instruments and data sources of sky brightness and weather variables; while Section 3 presents and discusses the resulting statistical and seasonal properties of the studied variables.

2. Data and Methodology

2.1. Astronomical Observatories in El Leoncito, Argentina

OAFA and its neighboring Complejo Astronómico el Leoncito (CASLEO[6]) are two of the best sites for astronomical observations in Argentina. Located $\sim$ 3 km apart in the Andes mountain chain at a height of $\sim$ 2500 m in El Leoncito National Park, OAFA and CASLEO have provided the necessary infrastructure to host both day and nighttime scientific facilities since their openings in 1960 and 1983, respectively. Notable past or present daytime instruments at CASLEO include the 1.5-m Solar Submillimeter Telescope (SST, Krucker et al., 2013) and The POlarization Emission of Millimeter Activity at the Sun (POEMAS, Valio et al., 2013) among others. Meanwhile, OAFA hosts the Mirror Coronagraph for Argentina (MICA, see Section 2.3), the H-alpha Solar Telescope for Argentina (HASTA, Francile et al., 2008, 2016), the 30-THz solar telescope (AR30T, López et al., 2022), and the High Altitude THz Solar Photometer (HATS, Giménez de Castro et al., 2020).

Some of the excellent daytime observing conditions in El Leoncito have been reported previously; e.g., Valle Silva et al. (2020) estimated a WV content below 5 mm using GHz measurements. Piacentini et al. (2016) and Freire et al. (2019) reported mean particle concentrations below 9 000 and 800 000 particles m^{-3} for sizes $>$5 and $>$0.5 μm, respectively. These dust levels are below the ISO class-8 cleanliness requirements, comparable to those shown in Table 1, and confirmed by the AERONET[7] station that operated at CASLEO, see

[3] See www2.hao.ucar.edu/cosmo.

[4] This includes three generations of white-light coronographs, MK-3 (1980 – 1999), MK-4 (1999 – 2013) and COSMO K-Cor (2013-present, see de Wijn et al., 2012).

[5] See exactas.unsj.edu.ar/investigacion/observatorio-astronomico-felix-aguilar-oafa/.

[6] See casleo.conicet.gov.ar/.

[7] See aeronet.gsfc.nasa.gov/cgi-bin/data_display_aod_v3?site=CASLEO&nachal=2&level=1&place_code=10.

Otero et al. (2013) for extra details. They also reported a yearly average precipitable WV of ~ 7 mm with a mean in July and August below 5 mm. In addition, Hurtado et al. (2022) have collected 20 years of the day- and nighttime sky conditions soon to be reported.

We present here the statistics of daytime sky brightness at the Carlos U. Cesco station (latitude 31° 48' 8.5" S, longitude 69° 19' 35.6" W, elevation 2370 m above mean sea level) in OAFA, derived from the auxiliary brightness detectors mounted on MICA, see Section 2.3. This information is complemented with weather data from two local weather stations (Section 2.2) and observation logs (Section 2.5).

2.2. Weather

Weather data is extracted from two local weather stations. The first one, belonging to the MASTER network (Mobile Astronomical System of TElescope-Robots[8]), registered relative humidity, ambient temperature, wind speed, and zenithal cloud temperature from 2012.02.08 to 2020.10.16 (3 173 days). The mean sampling interval is ≈ 1 min, resulting in a data set with 1 914 564 measurements acquired during 2 967 different days (94% of the operational interval).

The second weather station belongs to MICA and registered the same parameters as MASTER (except that it does not measure cloud temperature) from 2000.12.17 to 2018.02.21 (6 276 days). The mean sampling interval is ≈ 5 min, and the resulting data set contains 571 079 measurements acquired during 4 665 different days (74% of the operational interval).

We resample the MASTER data set to have also an interval of 5 min and keep from both data sets the measurements acquired between local 8:00 and 20:00 (timezone is UTC-3). In addition, we estimate the precipitable WV content from the surface relative humidity and temperature using the model described in Otárola et al. (2010).

2.3. Sky Brightness

MICA (Stenborg et al., 1999a) is a 4.7-cm mirror coronagraph with an almost identical design to the LASCO-C1 instrument (Brueckner et al., 1995) onboard the emblematic Solar and Heliospheric Observatory mission (SOHO, Domingo, Fleck, and Poland, 1995). MICA was built upon the experience gained with the ground-based prototype of LASCO-C1, named PICO (Epple and Schwenn, 1994), and produced low-coronal filtergrams from 1997 to 2012 at two well-known emission Iron lines (Fe XIV at 530.3 nm and Fe X at 637.4 nm) with a FOV of 1.05 to 2 $R_{\odot}$, e.g., Stenborg et al. (1999b), Stenborg, Schwenn, and Srivastava (1999), Balmaceda et al. (2003). Given MICA's sensitivity to the light scattered by the sky, the images acquired with the filters for the green (530.30 ± 0.15 nm) and red (637.40 ± 0.15 nm) lines are calibrated using a second pair of continuum images acquired close in time (~ 3 min) using a green (526.0 ± 1.0 nm) and a red (634.0 ± 1.0 nm) continuum filter, see Stenborg (2000) for extra details. The instrument spatial sampling is 3.7 arcsec, and the typical exposure times employed are in the 10 to 40 s range.

To perform robotic observations, MICA includes two auxiliary brightness detectors described below:

- Sun-T (Stenborg et al., 1999a; Stenborg, 2000): It detects the integrated white-light brightness of the solar disk (up to 2 $R_{\odot}$) using a photodiode model BPW20R with relative sensitivity of 1 at 920 nm, above 0.5 in the 550 – 1050 nm range, and above 0.1 in

[8] Available at observ.pereplet.ru/.

the 400 – 1100 nm range. Besides the expected air mass dependence, a low Sun-T brightness is associated with low sky transmission due to an increase in the content of WV associated with clouds and/or the presence of aerosols in the atmosphere.

- Sky-T (Epple, 1997; Stenborg, 2000): Is a small externally-occulted, refractive coronagraph that measures sky brightness integrated over a ring around the solar disc using a photodiode. A high-pass filter (RG590) sets the lower end of the spectral range to 590 nm while the diode (same model as Sun-T) sensitivity limits the response to 1100 nm. The instrument vignetting function extends from 3 to 12 $R_\odot$ and peaks at 7.2 $R_\odot$, resulting in 50% of the output signal coming from the 6.5 to 9.1 $R_\odot$ FOV. A low Sky-T brightness is related to either low sky transmission or low scattering. The former can be distinguished from the latter by a simultaneous reading of Sky-T. The output voltage of both Sun-T and Sky-T after digitalization ranges from 0 to 4.9 mV and has a resolution of 19.5 μV.

The robotic operation software of MICA decides if the conditions are suitable for coronal observations based on wind speed, and sky brightness and scattering measured by Sun-T and Sky-T, respectively. After years of operation, one threshold value for Sun-T (2 mV) and two values for Sky-T (1 and 2 mV) have been experimentally selected by the MICA team to classify the sky conditions based on the quality of the resulting coronal observations, see (Stenborg et al., 1999a). The resulting sky classes for transmission are Cloudy (Sun-T$\leq$ 2 mV) and Sunny (Sun-T$>$ 2 mV), while for coronal sky quality are Bad (Sky-T$>$ 2 mV), Moderate (1 mV$<$Sky-T$\leq$ 2 mV), and Good (Sky-T$\leq$ 1 mV). MICA acquired data only in Sunny-Moderate or Sunny-Good conditions.

We collect data from Sky-T and Sun-T covering the complete 15-year operational period of MICA, from 1997.12.01 to 2012.06.27 (5 323 days). After removing saturated and erroneous data, e.g., due to pointing errors in very cloudy conditions, the data set comprises 18 270 640 measurements acquired with a variable temporal sampling (see below), during 3 741 different days ($\sim$ 70% of MICA operational period). A sample set of measurements, corresponding to the same day (22 February) over 14 different years, is shown in Figure 1. Besides the expected dependence on the Sun zenith angle (airmass), there are occasional variations due to clouds. The latter are typically accompanied by an increase in atmospheric scattering, i.e., larger values of Sky-T. The most rapid fluctuations of brightness are related to the presence of thin, high altitude clouds, such as cirrus.

Given its operational purpose, Sky-T measurements are not normalized to the solar disk brightness. However, Sky-T and Sun-T have high cadence and a long measurement record with good temporal coverage, rendering them a valuable source to characterize the daytime sky over OAFA. Thus, to report normalized brightness measurements that are useful for comparison with the results of other site surveys, we make use of the correlation between the Sky-T/Sun-T ratio and simultaneous MICA measurements. The latter have lower cadence and worse time coverage because MICA observed only under good sky conditions (see above); however, they are normalized and expressed in ppm of the disc brightness. The MICA normalization procedure involves frequent calibration measurements of the solar disk brightness, i.e., the FOV is shifted to directly image the solar disk using a known neutral density disperser that avoids saturation and reduces coronal structures. As part of this procedure, a sky-brightness profile ($I_{\rm mica}$ in ppm of the disk center) of the form $I_{\rm mica} = k_0 + k_1 \times e^{k_2 r}$, where k_0, k_1, and k_2 are free parameters and r the radial distance to disk center, is fit to the radially averaged filtergrams. The MICA normalization and calibration procedures are detailed in Stenborg (2000), including a successful verification by comparing MICA images to quasi-simultaneous, calibrated measurements obtained with the 40-cm Sacramento Peak Emission Line Coronal Photometer (Smartt, 1982).

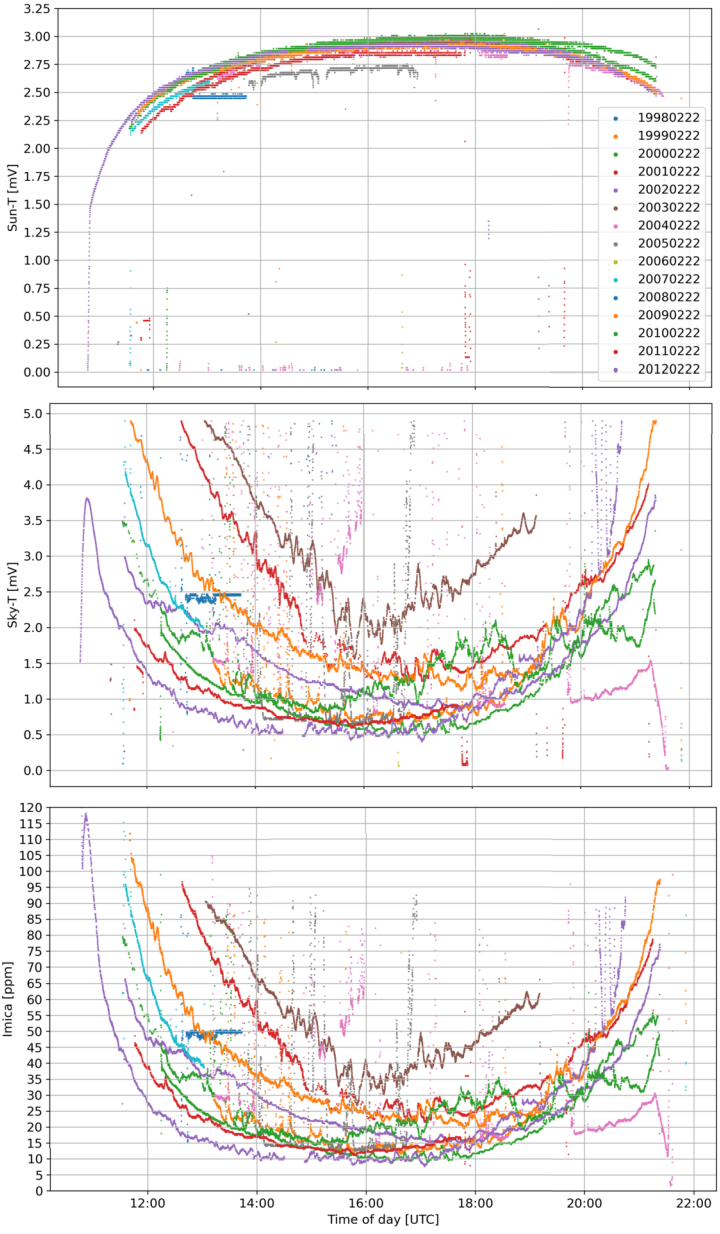

Figure 1 Example raw Sun-T (top panel) and Sky-T (middle panel) measurements for 22 February on 14 different years (see legend), presenting typical variations with airmass and transient clouds. We also show the corresponding continuum sky brightness values ($I_{\rm mica}$, bottom panel) estimated at 526.0 nm and 6 $R_\odot$. See the text for extra details.

We correlate the Sky-T/Sun-T ratio to the normalized sky brightness obtained at 6 $R_\odot$ from the radial brightness profile fitted to the green continuum MICA filtergrams (526.0 $\pm$ 1.0 nm). This is shown in Figure 2 for 1 367 different MICA measurements acquired during

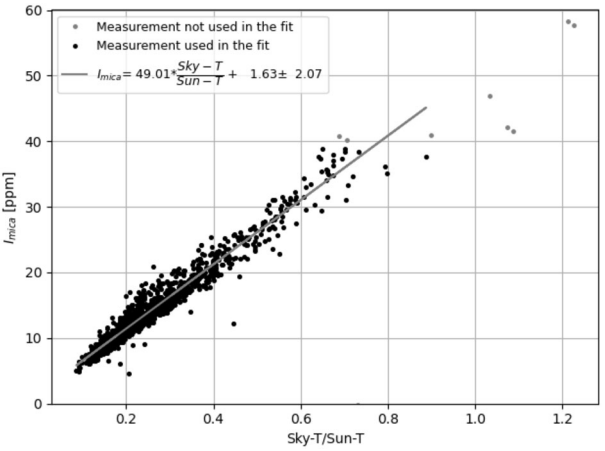

Figure 2 Correlation between calibrated MICA measurements in the continuum near the Fe XIV line at 526.0 nm (radially averaged and extrapolated to 6 $R_\odot$), versus the Sky-T/Sun-T ratio. We use the measurements below 40 ppm (black points) to fit the linear calibration expression (grey line) specified in the legend. The last term of the linear expression is the rms difference between the fit and the used measurements.

37 days, from 2004 to 2006, selected to include all seasons. Given that we are interested in characterizing more accurately the low sky brightness conditions, we fit a linear correlation to the measurement points that have $0 < I_{\rm mica} < 40$, see the legend of the same figure. The fitted linear relationship is used to estimate $I_{\rm mica}$ values from the measured Sky-T and Sun-T pairs for the complete data set, as exemplified in the bottom panel of Figure 1. For the rest of the paper, we use $I_{\rm mica}$ to denote the above-described sky brightness value estimated from the Sky-T/Sun-T ratio. Note that this linear relationship implies that the upper limit for the empirical sky conditions defined by the MICA team to operate the telescope corresponds approximately to 26 ppm$< I_{\rm mica} <$ 50 ppm for Sunny-Moderate and $I_{\rm mica} <$ 26 ppm for Sunny-Good conditions.

Different from the Evans and SBM photometers, an accurate and stable normalization of Sky-T is more difficult because the disk brightness is registered by Sun-T, which is a separate instrument with an independent entrance aperture, optical path, and detector. SBM is reported to be accurate down to 1 ppm, while our brightness estimations based on the above-mentioned linear correlation have an RMS error of ~ 2 ppm with respect to the value at 6 $R_\odot$, of the above-described fit to the radially averaged MICA continuum filtergram. Moreover, this error is likely larger for sky brightness above the 40 ppm limit used in Figure 2.

The contribution of instrumental scattered light to the sky brightness estimations can be roughly approximated using the zero-crossing term of a fit to the $I_{\rm mica}$ vs. airmass curve, as suggested by Martinez Pillet, Ruiz Cobo, and Vazquez (1990). We expect this value to be low, because the MICA images used in Figure 2 to derive the linear relationship are corrected for scattered light, as part of the MICA calibration procedure. The fitted function is $I_{\rm mica} = B + \alpha M(z,t)$, where B is the instrumental scattered light term, and $M(z,t)$ is the airmass as function of the solar zenith angle (z) and the thickness of the atmosphere (t). As done for the SBM calibration (Lin and Penn, 2004), we adopt a spherical atmosphere and use $M(z,t) = -R\cos(z) + \sqrt{R^2\cos^2(z) + 2tR + t^2}$, where R is the Earth radius plus the site altitude. This estimation of the instrumental scattered light is very sensitive to the atmospheric conditions and thus gives erroneous results, e.g., if the observed brightness before and after local noon considerably differ or if the curve is under sampled. For the case of SBM, these difficulties are reported by Lin and Penn (2004), Zhao et al. (2014) and Zhao et al. (2018), who derive the instrumental scattered light from the data of only few selected and very stable days. As done by Zhao et al. (2018), we fit only the measurements acquired

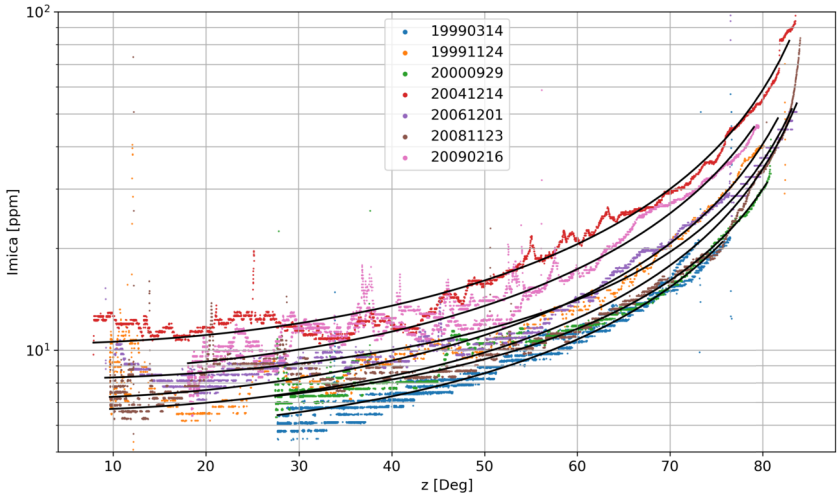

Figure 3 Sky brightness vs. zenith angle measured during 7 different stable days (see legend). The morning and after noon values for each day partially overlap. The fits (black lines) to the morning values are used to estimate the residual instrumental scatter light. Note that the vertical axis has a logarithmic scale.

before local noon. We start by grouping the brightness values of each day every $z = 1°$ and keep only the days where the RMS of 90% of these bins, each including measurements acquired both before and after noon, are below 2 ppm. This selection results in 176 fitted days with a median B of 3.0 ppm and a 0.1 quantile of 0.76 ppm. We further filter this group and keep only days that have at least 6 h of continuous measurements that include zenith angles ≥ 75 deg and have a fit RMS residual below 2 ppm. The 7 most stable days resulting from this second selection are shown in Figure 3 and have a median B of 0.8 ppm. We adopt a conservative approach and subtract from all of our brightness estimations an instrument scatter light term of 0.7 ppm.

Considering the fast sampling rate of Sky-T and Sun-T (mean of 3.7 s and 0.99 quantile of 16.0 s), we derive the total observed time from a daily zero-order interpolation of the I_{mica} time series. This is, the brightness level between two consecutive measurements of the same day is assumed constant and equal to the value observed in the first of the two measurements.

We estimate the expected number of annual hours for a given sky brightness range as done in Hill et al. (2006). Namely, we multiply the mean observed hours per year (the total observed hours divided by the number of observed years, N_{years}) at a given sky brightness range by $365 \times N_{\text{years}}/N_{\text{up}}$. Where N_{up} is the total number of days Sky-T and Sun-T were operational. Note that such correction is independent of the number of observed years, i.e. we consider an approximately homogeneous coverage of the observed years.

2.4. Clear Sky Time Fraction

We compute CSTF using the rapid variations of sky transmission observed in Sun-T data when clouds are present. This is analogous to the criterion adopted by the DKIST site selection team, see Section 1. We proceed as follows:

i) For each day, we divide the full observed period (from first to last measurement) in time bins, each lasting 5 min.

ii) To ensure a proper sampling density, we select days that have an observed period of at least 6 h, and that have at least 2 measurements in more than 90% of the 5-min time bins.
iii) We classify the time bins of each selected day into two categories. If the absolute difference between the min and max Sun-T value in the bin is larger than twice the resolution (± 19.5 μV), the bin is considered cloudy, i.e. the intensity change is not due to the air-mass change but likely produced by a cloud. Otherwise, the 5-min time bin is tagged as clear sky.
iv) The observed CSTF for each day is the ratio of the number of clear to the total number of time bins.

We also estimate the CSTF from another independent source. This is the value of the zenithal cloud temperature obtained from weather data (see Section 2.2). The cloud temperature of the MASTER weather station is obtained using the commercial Boltwood Cloud Sensor II, manufactured by Boltwood Systems Corporation and distributed by Diffraction Limited. This sensor registers integrated IR brightness in the zenith direction and the 8 to 14 μm spectral range. A clear sky presents a low cloud temperature, usually below $-25°$ C. However, while cloud temperature values are sensitive to large patches of thick clouds, they are less likely to detect thin haze or high cirrus clouds due to their low IR brightness. This is why Marchant, Smith, and Steele (2008) compute CSTF considering not only the mean cloud temperature but also its time variability. We follow their criterion and compute CSTF as done for Sun-T (see steps i top iv above), except that the criterion to classify each 5-min bin (step iii) is the following: If the mean value of Cloud Temperature is larger than $-25°$C or there are more than two measurements that deviate from the mean more than 1°C, the bin is tagged as cloudy. Otherwise, the time bin is tagged as clear sky.

2.5. Observing Logs

We analyze daily observing reports covering the full operational period of MICA and classify each day as follows:

- Observed clear day: Suitable weather conditions and MICA observations made.
- Observed cloudy day: Observers did not operate the telescope due to bad weather conditions.
- Not observed day: Lacks an observing report, mostly because there were no observations planned, or the telescope was not operational.

3. Results and Discussion

3.1. Weather

The main statistical properties of the daytime weather parameters obtained from the combined data set of the two meteorological stations described in Section 2.2 are summarized in Table 2 and presented in Figure 4. The weather data set has a high statistical relevance due to the long (20 years), multiseasonal time interval analyzed. Furthermore, this interval is well sampled, with 4 665 (64%) out of 7 244 days containing valid weather measurements. Note that around winter, from months 6 to 9, is the driest season. The median monthly temperature during this time is below 12°C, although the median daily thermal amplitude can be large ($\approx 15°$C). Moreover, the median precipitable WV in this season is below 5 mm,

Table 2 Summary of daytime weather conditions at OAFA in El Leoncito, Argentina. We show the min, median, and max values observed between local 8:00 and 20:00, see also Figure 4.

Parameter	El Leoncito
Time interval	2000.12.17 to 2020.10.16 (7 244 days)
Observed days	4 665
Valid data points	571 069
Sampling rate	5 min
Temperature [C°]	−29.9 ; 17.5 ; 42.3
Humidity [%]	1.0 ; 24.0 ; 146.0
Wind speed [$m\,s^{-1}$]	0.1 ; 2.6 ; 49.6
Precipitable water vapor [mm]	0.0 ; 5.8 ; 39.3
Atmospheric pressure [mm Hg]	262.8 ; 570.0 ; 687.2

reaching a minimum of 3.2 mm in August, see Figure 4, which is in line with previous results (e.g., Piacentini et al., 2016). As a comparison, the sky over one of the driest observatories in the world, Cerro Armazones in the Chilean Atacama desert, presents a median WV of 2.87 mm (Otárola et al., 2010). This low WV considerably benefits observations at infra-red wavelengths by reducing atmospheric absorption and dispersion; e.g., one of the DKIST site requirements is to have WV below 5 mm for at least 20% of the best observing time.

The median wind speed of 2.6 $m\,s^{-1}$ (9.36 $km\,h^{-1}$) is lower than the values measured at the observatories listed in Table 1, although the highest speed registered in OAFA reached 49.6 $m\,s^{-1}$ (179 $km\,h^{-1}$). The preferred wind direction is west, from the Andes mountains. The fastest wind gusts are generally related to episodes of Zonda, a warm and very dry wind associated with adiabatic compression upon descending the eastern slopes of the Andes (see, e.g., Norte, 2015). We note that the yearly median wind speeds measured by the MASTER weather station, starting in 2012, are larger. Besides a contribution from a calibration bias, the difference can be due to their different exact locations within OAFA relative to the various buildings and detailed topographic profiles.

3.2. Sky Brightness

Table 3 summarizes the results of the estimated sky brightness at OAFA. In addition, the seasonal, yearly, and main statistical characteristics derived using the methodology described in Section 2.3 are presented in Figure 5. These results are of statistical relevance both because of the 15-year long, multiseasonal time interval analyzed, as well as the good sampling, i.e., 70% of the days have observations. The most important aspects of the brightness values found are summarized and discussed below:

- The median value of the observed brightness we found at OAFA, 15.8 ppm, is comparable to the values measured at the Big Bear and Roque de los Muchachos observatories. Recall that the closest values reported in Table 1 are measured at 530 nm, while we estimate brightness at 526.0 nm. On the other hand, the skies of the Hawaiian observatories are darker by a factor of ≈ 5. Note that, when measuring very low brightness values, the correct estimation of the instrumental scatter light term becomes critical.
- Regarding seasonal changes, the darker skies are found in winter, the driest season. In phase with the seasonal rainfall, the minimum brightness occurs in months 6 and 7. This

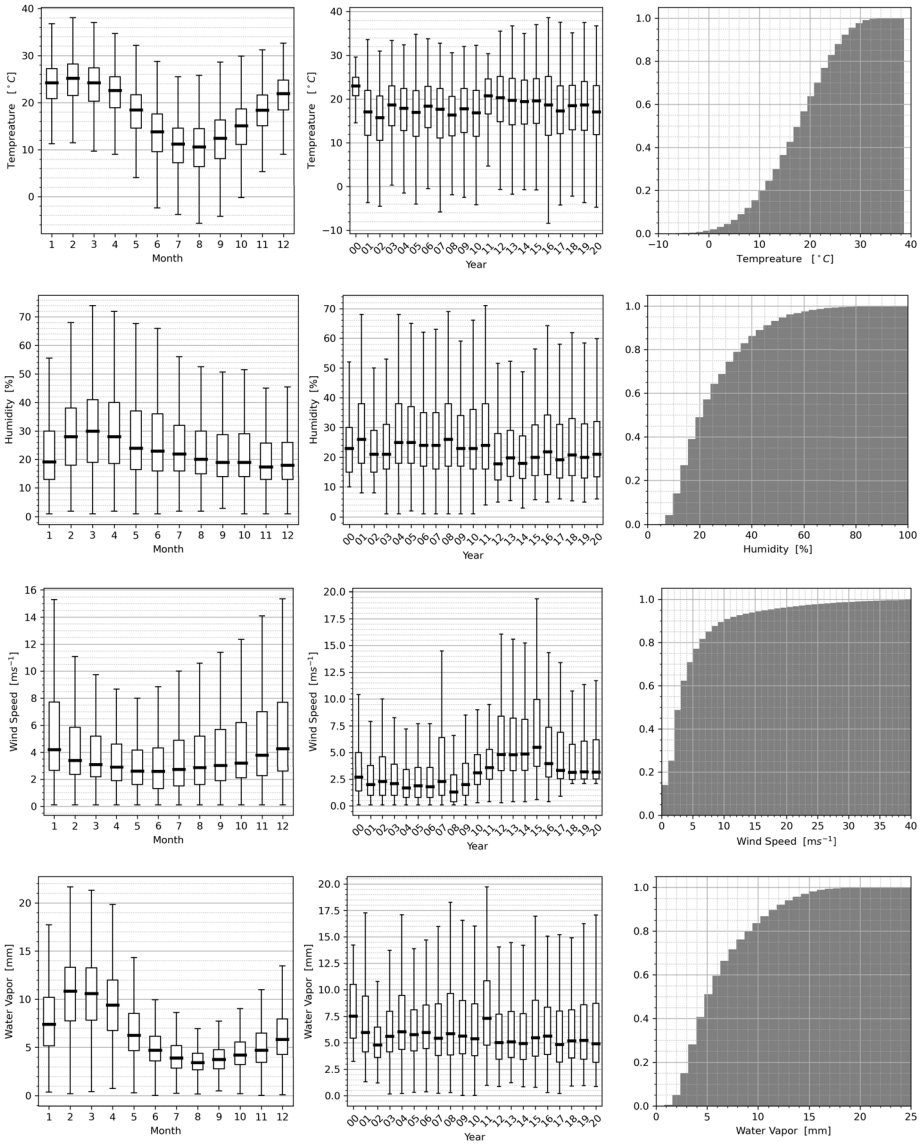

Figure 4 Seasonal and yearly statistics of the main daytime weather parameters at OAFA in El Leoncito, Argentina. We show monthly (panels in the left column) and yearly (panels in the middle column covering from the year 2000 to 2020) box plots for various weather parameters (panels in each row, see the vertical axes titles). Each box extends from the lower to the upper quartile with a black line at the median. The whiskers extend from 0.05 to 0.95 quantiles to illustrate the data range. We also include the cumulative histograms normalized to the total observed time (panels in the right column). See text for extra details.

is about one month out of phase with respect to the minimum of our estimated precipitable WV content, see Figure 4. After winter, when spring starts in the southern hemisphere (21 September), sky brightness rises mostly due to the increase in cloud frequency. The exact contribution of dust and organic particles to the increase in brightness in this season is

Table 3 Summary of day sky brightness measurements at OAFA in El Leoncito, Argentina. We show the observed median brightness, including all valid data points, estimated at 526.0 nm and 6 $R_{\odot}$. As a reference, see Table 1.

Parameter	El Leoncito
Time interval	1997.12.01 to 2012.06.27 (5, 323 days)
Observed days	3 741
Observed hours	25 376
Valid data points	18 270 640
Mean sampling rate	3.7 s
Median sky brightness	15.8 ppm

unknown. Stenborg (2000) reports flying Aspen tree seeds detected in a few MICA observations. In addition, spring is the season with more frequent episodes of the dusty Zonda wind (see above). Note that, there are 10 months per year where 25% of the observed brightness values are below 11 ppm. Likewise, from months 4 to 12, at least 5% of the observed values are below ~ 6 ppm.

- Regarding the observed yearly brightness changes, as only a few other studies suggest, we notice a (mild) correlation with the solar cycle. Namely, the larger the sunspot number, the darker the sky, see (e.g., Sakurai, 2002) for extra details. The larger median brightness of 2012 can be attributed to two reasons. Firstly, only the brighter months (1 to 6) were measured, leading to selection bias. Secondly, there may be a contribution from the large eruption of the Puyehue-Cordón Caulle volcanic complex (e.g., Balseiro et al., 2014). Even though the complex is about 1 000 km south, its eruption released ashes from June 2011 to March 2012, which dispersed in large portions of Argentina and even circled the globe (Klüser, Erbertseder, and Meyer-Arnek, 2013).
- The 25 379 hours of observation represent 56% of the total sunshine hours. The observed brightness histogram peaks at the 8 – 9 ppm bin, with almost 1 000 total hours observed in this range.
- The cumulative distribution of the number of annual hours at each brightness value indicates that there is an expected 1 050 hours per year with sky brightness below 20 ppm.

3.3. Clear Sky Time Fraction

The resulting estimations of CSTF per day using two different proxies, Cloud Temperature, and Sun-T, are summarized in Table 4. In this Table, we denote, with observed days, the number of days that fulfill the criteria detailed in Section 2.4. Note that, while both estimations of the median CSTF differ, they are large and comparable to the sites presented in Table 1. The difference in our estimations may be because we do not make an extrapolation from the observed CSTF to the expected one, i.e. we assume the number of observed days is large enough and the sampling uncorrelated to the cloud coverage conditions, to get a representative sample of the full statistical population. The no correlation assumption is more valid for the CSTF estimation based on Cloud temperature because the weather station operates 24 h per day. Our results are also in line with the night-time cloud coverage estimation done by Martinis et al. (2013) at CASLEO. They found that the night sky is clear 75 to 80% of the time, with no pronounced seasonal changes. On the other hand, we find a strong seasonal variation of the CSTF estimated from cloud temperature, see Figure 6. As explained above, winter is the driest season, and thus a lower cloud presence is expected. Our estimated monthly median peaks a month earlier, reaching 0.86 in May.

In Table 4, we also include the results of the daily observing logs classification presented in Section 2.5. We find that, out of the 4 099 days with an observing report, 3 525 (86%) are

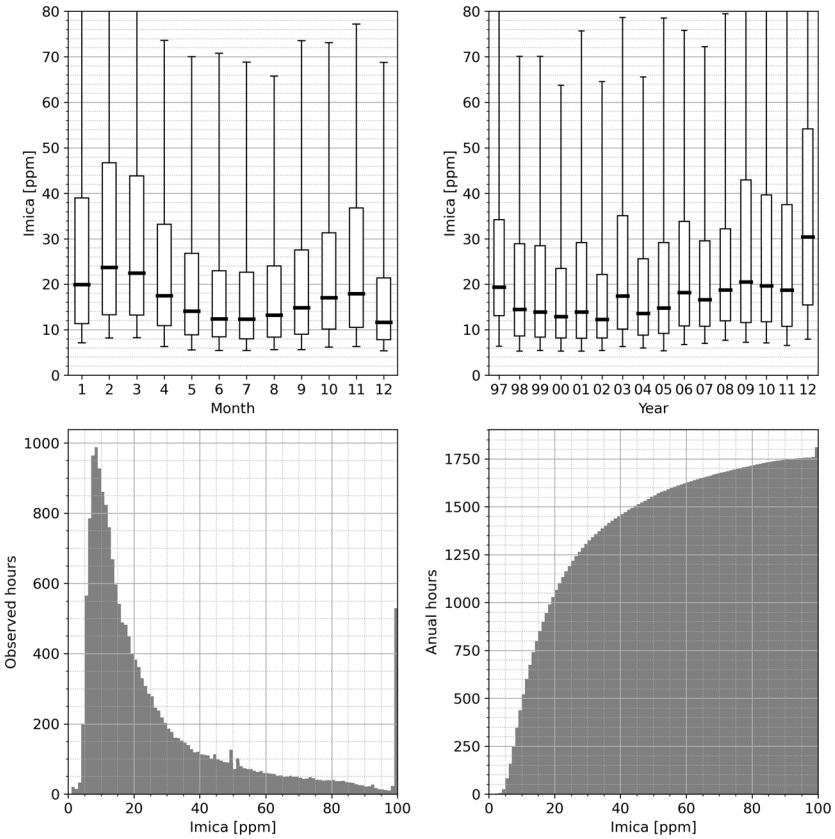

Figure 5 Estimated daytime sky brightness statistics at OAFA in El Leoncito, Argentina. We show monthly (top left) and yearly (top right) box plots. Each box extends from the lower to the upper quartile with a black line at the median. The whiskers extend from 0.05 to 0.95 quantiles to illustrate the data range. We also present the brightness distribution considering the total observed hours (bottom left), and the cumulative distribution considering the expected annual hours (bottom right). The bin width is 1 ppm, while the last bin includes all values above 99 ppm. See Table 3 for extra details.

classified as clear days. This result is statistically significant, given that 77% of the days in the analyzed time interval have an observing report. Note that the fraction of clear days is a different quantity than the CSTF because the former only considers if the sky conditions were suitable to perform a MICA observation, not accounting for the duration of the clear conditions during the day.

4. Conclusions

We have characterized the daytime sky quality at the Carlos Ulrico Cesco station of the OAFA observatory in El Leoncito, Argentina, in terms of typical weather variables, sky brightness, and CSTF. The weather statistics are comparable to those found in other desertic, high-altitude observatories, see Table 2. The seasonal variability (Figure 4) is dominated by the dry winter ($WV < 5$ mm) where the sky is mostly clear, see below. The most extreme

Table 4 Clear sky time (and days) fraction at OAFA in El Leoncito, Argentina, estimated from different sources. The first two sources are used to compute independent estimations of the median CSTF. On the other hand, the observing logs allow computing the fraction of clear days. See the text for extra details.

Parameter	El Leoncito
Source: Cloud Temperature	
Time interval	2012.02.08 to 2020.10.16 (3 173 days)
Observed days	2 872 (91%)
Median clear sky time fraction	0.67
Source: Sun-T	
Time interval	1997.12.02 to 2012.06.27 (5 322 days)
Observed days	1 296 (24%)
Median clear sky time fraction	0.74
Source: Observing logs	
Time interval	1997.12.01 to 2012.06.27 (5 323 days)
Observed days	4 099 (77%)
Clear days fraction	0.86

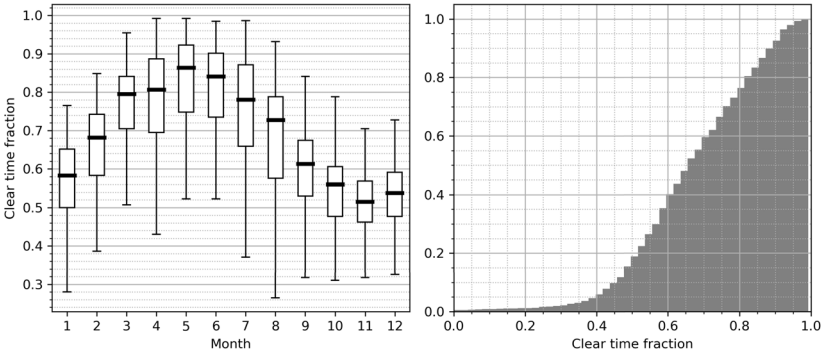

Figure 6 Daytime clear sky time fraction at OAFA in El Leoncito, Argentina, estimated from cloud temperature. We show a monthly box plot (left). Each box extends from the lower to the upper quartile with a black line at the median. The whiskers extend from 0.05 to 0.95 quantiles. We also present the normalized cumulative distribution of the observed days (right). See the text for extra details.

weather conditions include temperatures down to ≈ -30°C and up to ≈ 43°C, daily thermal amplitudes up to ≈ 15°C, and very rare but fast ($\approx 50\ \mathrm{m\,s^{-1}}$) wind gusts, likely related to events of the hot local Zonda wind.

The median sky brightness, estimated at 526.0 ± 1.0 nm and 6 solar radii from the solar disk center, is found to be 15.8 ppm, with the minimum values taking place during the dry winter (monthly median during May–August is below 14.0 ppm). Moreover, there are 10 months per year where 25% of the observed values are below 11 ppm, see Table 3 and Figure 5. A basic correction for downtime allows us to estimate that 1 050 hours per year are expected to have sky brightness below 20 ppm. We note that our results are less accurate than a possible direct normalized measurement, which could be acquired by a dedicated sky brightness monitor, such as the SBM (see Section 2.3).

The more conservative estimation of CSTF using the cloud temperature data yields a median of 0.67, being above ≈ 0.8 from March to June, see Table 4 and Figure 6. On the other hand, 86% of the days that have an observing log (77% of the total number of days in

the studied interval) are classified as clear days when coronal measurements were acquired using MICA, see Table 4.

The weather variables, low sky brightness, and high CSFT values found in OAFA are comparable to the levels found among the best astronomical observing sites in the world. This renders the el Leoncito area, including the OAFA and CASLEO observatories, an excellent candidate for the allocation of future daytime astronomical instrumentation.

Acknowledgments FAI and HC are members of the "Carrera del Investigador Científico" of CONICET. We thank Dr. Fernando López for useful discussions and the algorithm to compute water vapor content; Mr. Gabriel Zucarelli for his help with data processing; and Dr. German Cristiani and the "Instituto de Astrofisica del Espacio" (IAFE) for helping with MICA data collection.

Author contributions F.I. wrote the main manuscript text, F.C. processed weather data and prepared Figure 4. F.I., C.F., J.L., H.C. and L.B. collected and analyzed the data. All authors reviewed the manuscript.

Funding FAI and HC are members of the "Carrera del Investigador Científico" of CONICET, and supported by projects MSTCAME0008181TC (UTN) and PIP11220200102710CO (CONICET). FAI and FC are supported by The Max Planck Partner Group between the University of Mendoza and the Max Planck Institute for Solar System Research (MPS). CF acknowledges support from CICITCA UNSJ.

Data Availability This work uses data obtained in the framework of the German Argentinean MICA Project at OAFA, a collaborative effort between IAFE, OAFA, and MPS. For data inquiries contact the authors.

Declarations

Competing interests The authors declare no competing interests.

References

Balmaceda, L., Dal Lago, A., Stenborg, G., Francile, C., Gonzalez, W.D., Schwenn, R.: 2003, Continuous tracking of CMEs using MICA, and LASCO C2 and C3 coronagraphs. *Adv. Space Res.* **32**(12), 2625. DOI. ADS.

Balseiro, E., Souza, M.S., Serra Olabuenaga, I., Wolinski, L., Bastidas Navarro, M., Laspoumaderes, C., Modenutti, B.: 2014, Effect of the puyehue-cordon caulle volcanic complex eruption on crustacean zooplankton of andean lakes. *Ecol. Austral* **24**(1), 75. DOI. https://ojs.ecologiaaustral.com.ar/index.php/Ecologia_Austral/article/view/39.

Baumbach, S.: 1937, Strahlung, Ergiebigkeit und Elektronendichte der Sonnenkorona. *Astron. Nachr.* **263**(6), 121. DOI. ADS.

Brueckner, G.E., Howard, R.A., Koomen, M.J., Korendyke, C.M., Michels, D.J., Moses, J.D., Socker, D.G., Dere, K.P., Lamy, P.L., Llebaria, A., Bout, M.V., Schwenn, R., Simnett, G.M., Bedford, D.K., Eyles, C.J.: 1995, The Large Angle Spectroscopic Coronagraph (LASCO). *Solar Phys.* **162**, 357. DOI.

de Wijn, A.G., Burkepile, J.T., Tomczyk, S., Nelson, P.G., Huang, P., Gallagher, D.: 2012, Stray light and polarimetry considerations for the COSMO K-Coronagraph. In: Stepp, L.M., Gilmozzi, R., Hall, H.J. (eds.) *Ground-Based and Airborne Telescopes IV*, *Society of Photo-Optical Instrumentation Engineers (SPIE) Conference Series* **8444**, 84443N. DOI. ADS.

Domingo, V., Fleck, B., Poland, A.I.: 1995, The SOHO mission: an overview. *Solar Phys.* **162**, 1. DOI. ADS

Eldridge, R.G.: 1967, Water vapor absorption of visible and near infrared radiation. *Appl. Opt.* **6**(4), 709. DOI. http://opg.optica.org/ao/abstract.cfm?URI=ao-6-4-709.

Engvold, O.: 1991, Large Earth-based Solar Telescope-LEST. *Adv. Space Res.* **11**(5), 157. DOI. ADS.

Epple, A.: 1997, Erdgebundene beobachtungen der sonnenkorona mit einem spiegelkoronagraphen. PhD thesis, University of Goettingen.

Epple, A., Schwenn, R.: 1994, PICO - a mirror coronograph on Pic Du Midi. In: Hunt, J.J. (ed.) *Solar Dynamic Phenomena and Solar Wind Consequences, the Third SOHO Workshop*, *ESA Special Publication* **373**, 399. ADS.

Evans, J.W.: 1948, A photometer for measurement of sky brightness near the sun. *J. Opt. Soc. Am.* **38**(12), 1083. DOI. http://opg.optica.org/abstract.cfm?URI=josa-38-12-1083.

Fang, C.: 2011, Recent progress of solar physics research in China. *Res. Astron. Astrophys.* **11**(12), 1377. DOI. ADS.

Francile, C., Castro, J.I., Leuzzi, L., Luoni, M.L., Rovira, M.G., Cornudella, A., Gómez, W., Sarmiento, R.: 2008, New observational capabilities of the H-alpha Solar Telescope for Argentina (HASTA). *Bol. Asoc. Argent. Astron.* **51**, 339. ADS.

Francile, C., López, F.M., Cremades, H., Mandrini, C.H., Luoni, M.L., Long, D.M.: 2016, Moreton and EUV waves associated with an X1.0 flare and CME ejection. *Solar Phys.* **291**(11), 3217. DOI. ADS.

Freire, M.M., Della Ceca, L.S., Micheletti, M.I., Novara, I., García, B., Mancilla, A., Salum, G.M., Crinó, E., Piacentini, R.D.: 2019, Site analysis in the Argentinean Andean region for the placement of astrophysical observatories and solar photovoltaic power plants. The case of the "Leoncito 2" site. *Adv. Space Res.* **64**(2), 551. DOI. ADS.

Garcia, C.J., Yasukawa, E.A.: 1983, Mauna loa sky conditions – bench mark and present. *Publ. Astron. Soc. Pac.* **95**, 520. DOI.

Giménez de Castro, C.G., Raulin, J.-P., Valio, A., Alaia, G., Alvarenga, V., Bortolucci, E.C., Fernandes, S.H., Francile, C., Giorgetti, T., Kudaka, A.S., López, F.M., Marcon, R., Marun, A., Zaquela, M.: 2020, HATS: a ground-based telescope to explore the THz domain. *Solar Phys.* **295**(4), 56. DOI. ADS.

Giovanelli, R., Darling, J., Henderson, C., Hoffman, W., Barry, D., Cordes, J., Eikenberry, S., Gull, G., Keller, L., Smith, J.D., Stacey, G.: 2001, The optical/infrared astronomical quality of high Atacama sites. II. Infrared characteristics. *Publ. Astron. Soc. Pac.* **113**(785), 803. DOI. ADS.

Hill, F., Fischer, G., Grier, J., Leibacher, J.W., Jones, H.B., Jones, P.P., Kupke, R., Stebbins, R.T.: 1994a, The global oscillation network group site survey - part one. *Solar Phys.* **152**(2), 321. DOI. ADS.

Hill, F., Fischer, G., Forgach, S., Grier, J., Leibacher, J.W., Jones, H.P., Jones, P.B., Kupke, R., Stebbins, R.T., Clay, D.W., Ingram, R.E.L., Libbrecht, K.G., Zirin, H., Ulrichi, R.K., Websteri, L., Hieda, L.S., Labonte, B.J., Lu, W.M.T., Sousa, E.M., Garcia, C.J., Yasukawa, E.A., Kennewell, J.A., Cole, D.G., Zhen, H., Su-Min, X., Bhatnagar, A., Ambastha, A., Al-Khashlan, A.S., Abdul-Samad, M.-S., Benkhaldoun, Z., Kadiri, S., Sánchez, F., Pallé, P.L., Duhalde, O., Solis, H., Saá, O., González, R.: 1994b, The global oscillation network group site survey - part two. *Solar Phys.* **152**(2), 351. DOI. ADS.

Hill, F., Beckers, J., Brandt, P., Briggs, J., Brown, T., Brown, W., Collados, M., Denker, C., Fletcher, S., Hegwer, S., Horst, T., Komsa, M., Kuhn, J., Lecinski, A., Lin, H., Oncley, S., Penn, M., Radick, R., Rimmele, T., Socas-Navarro, H., Streander, K.: 2006, Site testing for the advanced technology solar telescope. In: Stepp, L.M. (ed.) *Society of Photo-Optical Instrumentation Engineers (SPIE) Conference Series*, *Society of Photo-Optical Instrumentation Engineers (SPIE) Conference Series* **6267**, 62671T. DOI. ADS.

Hurtado, S., Blázquez, J., Faifer, F., Pereyra, P.F., Cellone, S.A., Aballay, J.L., Antico, P.L., Giménez, M.A., Mammana, L.A., Ostrov, P.G., Reynaldi, M.V., Zaninelli, P.: 2022, Astro-meteorological characterization of CASLEO sites: technical description and evaluation of the data series. *Bol. Asoc. Argent. Astron.* **63**, 299. ADS.

Judge, P.G., Casini, R., Tomczyk, S., Edwards, D.P., Francis, E.: 2001, Coronal Magnetometry: a Feasibility Study. Technical report. ADS.

Klüser, L., Erbertseder, T., Meyer-Arnek, J.: 2013, Observation of volcanic ash from puyehue-cordon caulle with iasi. *Atmos. Meas. Tech.* **6**(1), 35. DOI. https://amt.copernicus.org/articles/6/35/2013/.

Krucker, S., Giménez de Castro, C.G., Hudson, H.S., Trottet, G., Bastian, T.S., Hales, A.S., Kašparová, J., Klein, K.-L., Kretzschmar, M., Lüthi, T., Mackinnon, A., Pohjolainen, S., White, S.M.: 2013, Solar flares at submillimeter wavelengths. *Astron. Astrophys. Rev.* **21**, 58. DOI. ADS.

Landi, E., Habbal, S.R., Tomczyk, S.: 2016, Coronal plasma diagnostics from ground-based observations. *J. Geophys. Res.* **121**(9), 8237. DOI. ADS.

Leibacher, J.W.: 1999, The global oscillation network group (GONG) project. *Adv. Space Res.* **24**(2), 173. DOI. ADS.

Liberatore, A., Capobianco, G., Fineschi, S., Massone, G., Zangrilli, L., Susino, R., Nicolini, G.: 2022, Sky brightness evaluation at Concordia Station, Dome C, Antarctica, for ground-based observations of the Solar Corona. *Solar Phys.* **297**(3), 29. DOI. ADS.

Lin, H., Penn, M.J.: 2004, The advanced technology solar telescope site survey sky brightness monitor. *Publ. Astron. Soc. Pac.* **116**(821), 652. DOI. ADS.

Liu, Y., Shen, Y.-D., Zhang, X.-F., Liu, N.-P.: 2012, Using a new sky brightness monitor to observe the Annular Solar Eclipse on 15 January 2010. *Solar Phys.* **279**(2), 561. DOI. ADS.

López, F.M., Giménez de Castro, C.G., Mandrini, C.H., Simões, P.J.A., Cristiani, G.D., Gary, D.E., Francile, C., Démoulin, P.: 2022, A solar flare driven by thermal conduction observed in mid-infrared. *Astron. Astrophys.* **657**, A51. DOI. ADS.

Lyot, B., Marshall, R.K.: 1933, The Study of the Solar Corona without an Eclipse. *J. Roy. Astron. Soc. Can.* **27**, 225. ADS.

Marchant, J., Smith, R.J., Steele, I.A.: 2008, Calibration of the boltwood cloud sensor. In: Stepp, L.M., Gilmozzi, R. (eds.) *Ground-Based and Airborne Telescopes II*, *Society of Photo-Optical Instrumentation Engineers (SPIE) Conference Series* **7012**, 70123U. DOI. ADS.

Martinez Pillet, V., Ruiz Cobo, B., Vazquez, M.: 1990, Stray-light measurements at the Observatorio del Teide. *Solar Phys.* **125**(2), 211. DOI. ADS.

Martinis, C., Wilson, J., Zablowski, P., Baumgardner, J., Aballay, J.L., Garcia, B., Rastori, P., Otero, L.: 2013, A new method to estimate cloud cover fraction over El Leoncito Observatory from an all-sky imager designed for upper atmosphere studies. *Publ. Astron. Soc. Pac.* **125**(923), 56. DOI. ADS.

Norte, F.A.: 2015, Understanding and forecasting zonda wind (andean foehn) in Argentina: a review. *Atmos. Climate Sci.* **5**, 163. DOI.

Oakley, P.: 2015, Enclosure and site requirements document. (cosmolc-rq-6012). Technical report, High Altitude Observatory of the National Center for Atmospheric research.

Otárola, A., Travouillon, T., Schöck, M., Els, S., Riddle, R., Skidmore, W., Dahl, R., Naylor, D., Querel, R.: 2010, Thirty meter telescope site testing X: precipitable water vapor. *Publ. Astron. Soc. Pac.* **122**(890), 470. DOI. ADS.

Otero, L., Ristori, P., D'Elía, R., Pallotta, J., Quel, E.: 2013, Study of Casleo Clear Sky Aerosol Loads in 2011 from One Year of Aeronet Quality Assured Data. arXiv.

Penn, M.J., Lin, H., Schmidt, A.M., Gerke, J., Hill, F.: 2004, Extinction and sky brightness at two solar observatories. *Solar Phys.* **220**(1), 107. DOI. ADS.

Piacentini, R.D., García, B., Micheletti, M.I., Salum, G., Freire, M., Maya, J., Mancilla, A., Crinó, E., Mandat, D., Pech, M., Bulik, T.: 2016, Selection of astrophysical/astronomical/solar sites at the Argentina East Andes range taking into account atmospheric components. *Adv. Space Res.* **57**(12), 2559. DOI. ADS.

Quintero Noda, C., Schlichenmaier, R., Bellot Rubio, L.R., Löfdahl, M.G., et al.: 2022, The European Solar Telescope. *Astron. Astrophys.* **666**, A21. DOI. ADS.

Rimmele, T.R., Warner, M., Keil, S.L., Goode, P.R., Knölker, M., Kuhn, J.R., Rosner, R.R., McMullin, J.P., Casini, R., Lin, H., Wöger, F., von der Lühe, O., Tritschler, A., Davey, A., de Wijn, A., Elmore, D.F., Fehlmann, A., Harrington, D.M., Jaeggli, S.A., Rast, M.P., Schad, T.A., Schmidt, W., Mathioudakis, M., Mickey, D.L., Anan, T., Beck, C., Marshall, H.K., Jeffers, P.F., Oschmann, J.M., Beard, A., Berst, D.C., Cowan, B.A., Craig, S.C., Cross, E., Cummings, B.K., Donnelly, C., de Vanssay, J.-B., Eigenbrot, A.D., Ferayorni, A., Foster, C., Galapon, C.A., Gedrites, C., Gonzales, K., Goodrich, B.D., Gregory, B.S., Guzman, S.S., Guzzo, S., Hegwer, S., Hubbard, R.P., Hubbard, J.R., Johansson, E.M., Johnson, L.C., Liang, C., Liang, M., McQuillen, I., Mayer, C., Newman, K., Onodera, B., Phelps, L., Puentes, M.M., Richards, C., Rimmele, L.M., Sekulic, P., Shimko, S.R., Simison, B.E., Smith, B., Starman, E., Sueoka, S.R., Summers, R.T., Szabo, A., Szabo, L., Wampler, S.B., Williams, T.R., White, C.: 2020, The Daniel K. Inouye Solar Telescope - observatory overview. *Solar Phys.* **295**(12), 172. DOI. ADS.

Rouppe van der Voort, L., De Pontieu, B., Scharmer, G.B., de la Cruz Rodríguez, J., Martínez-Sykora, J., Nóbrega-Siverio, D., Guo, L.J., Jafarzadeh, S., Pereira, T.M.D., Hansteen, V.H., Carlsson, M., Vissers, G.: 2017, Intermittent reconnection and plasmoids in UV bursts in the Low solar atmosphere. *Astrophys. J. Lett.* **851**(1), L6. DOI. ADS.

Sakurai, T.: 2002, Eleven-year solar cycle periodicity in sky brightness observed at Norikura, Japan. *Earth Planets Space* **54**, 153. DOI. ADS.

Schmidt, D., Beard, A., Ferayorni, A., Gregory, S., Johnson, L., Marino, J., Rimmele, L., Rimmele, T.: 2021, Adding multi-conjugate adaptive optics to the Daniel K. Inouye Solar Telescope. In: Schreiber, L., Schmidt, D., Vernet, E. (eds.) *Adaptive Optics Systems VII* **11448**, SPIE, Bellingham, 114480F. International Society for Optics and Photonics. DOI.

Smartt, R.N.: 1982, Solar corona photoelectric photometer using mica etalons. In: *Instrumentation in Astronomy IV*, *Society of Photo-Optical Instrumentation Engineers (SPIE) Conference Series* **331**, 442. DOI. ADS.

Stenborg, G., Schwenn, R., Srivastava, N.: 1999, MICA observations of coronal transients. In: Vial, J.-C., Kaldeich-Schü, B. (eds.) *8th SOHO Workshop: Plasma Dynamics and Diagnostics in the Solar Transition Region and Corona*, *ESA Special Publication* **446**, 627. ADS.

Stenborg, G.A.: 2000, Interpretation and analysis on various time scales of narrow-band coronal oberservations obtained with a new coronagraph system. PhD thesis, Georg August University of Gottingen, Germany. ADS.

Stenborg, G., Schwenn, R., Srivastava, N., Inhester, B., Podlipnik, B., Rovira, M., Francile, C.: 1999a, MICA: the mirror coronagraph for Argentina. *Space Sci. Rev.* **87**, 307. DOI. ADS.

Stenborg, G., Schwenn, R., Srivastava, N., Inhester, B., Podlipnik, B., Rovira, M., Francile, C.: 1999b, Recent observations of the solar corona with a new ground-based coronagraph in Argentina (MICA). In: Habbal, S.R., Esser, R., Hollweg, J.V., Isenberg, P.A. (eds.) *Solar Wind Nine*, *American Institute of Physics Conference Series* **471**, 561. DOI. ADS.

Steven Tomczyk, P.O., Nelson, P.G.: 2015, Site evaluation and selection. (cosmolc-de-7400). Technical report, High Altitude Observatory of the National Center for Atmospheric research.

Suzuki, T., Miura, N., Kuwamura, S., Oya, S., Ueno, S., Nakatani, Y., Ichimoto, K.: 2018, Parallel processing of solar image restoration with phase diversity technique. In: Close, L.M., Schreiber, L., Schmidt, D. (eds.) *Adaptive Optics Systems VI*, *Society of Photo-Optical Instrumentation Engineers (SPIE) Conference Series* **10703**, 1070332. DOI. ADS.

Tomczyk, S., McIntosh, S.W., Keil, S.L., Judge, P.G., Schad, T., Seeley, D.H., Edmondson, J.: 2007, Alfvén waves in the solar corona. *Science* **317**(5842), 1192. DOI. ADS.

Tomczyk, S., Card, G.L., Darnell, T., Elmore, D.F., Lull, R., Nelson, P.G., Streander, K.V., Burkepile, J., Casini, R., Judge, P.G.: 2008, An instrument to measure coronal emission line polarization. *Solar Phys.* **247**(2), 411. DOI. ADS.

Tomczyk, S., Landi, E., Burkepile, J.T., Casini, R., DeLuca, E.E., Fan, Y., Gibson, S.E., Lin, H., McIntosh, S.W., Solomon, S.C., Toma, G., Wijn, A.G., Zhang, J.: 2016, Scientific objectives and capabilities of the Coronal Solar Magnetism Observatory. *J. Geophys. Res.* **121**(8), 7470. DOI. ADS.

Valio, A., Kaufmann, P., Giménez de Castro, C.G., Raulin, J.-P., Fernandes, L.O.T., Marun, A.: 2013, POlarization Emission of Millimeter Activity at the Sun (POEMAS): new circular polarization solar telescopes at two millimeter wavelength ranges. *Solar Phys.* **283**(2), 651. DOI. ADS.

Valle Silva, J.F., Giménez de Castro, C.G., Passarelli, C., Cornejo Espinoza, D., Cassiano, M.M., Raulin, J.-P., Valio, A.: 2020, Optical depth measurements at 45 and 90 GHz in CASLEO. *J. Atmos. Solar-Terr. Phys.* **199**, 105214. DOI. ADS.

van de Hulst, H.C.: 1953, The chromosphere and the corona. In: Kuiper, G.P. (ed.) *The Sun*, 207. ADS.

Yang, Z., Bethge, C., Tian, H., Tomczyk, S., Morton, R., Del Zanna, G., McIntosh, S.W., Karak, B.B., Gibson, S., Samanta, T., He, J., Chen, Y., Wang, L.: 2020, Global maps of the magnetic field in the solar corona. *Science* **369**(6504), 694. DOI. ADS.

Zhao, M.Y., Liu, Y., Elmhamdi, A., Kordi, A.S., Al-trabulsy, H.A., Zhang, X.F., Song, T.F., Liu, S.Q., Shen, Y.D., Tian, Z.J., Miao, Y.H.: 2014, Automatic data analysis for the Sky Brightness Monitor. *Mon. Not. Roy. Astron. Soc.* **443**(3), 1955. DOI. ADS.

Zhao, M.Y., Liu, Y., Elmhamdi, A., Kordi, A.S., Zhang, X.F., Song, T.F., Tian, Z.J.: 2018, Conditions for coronal observations at the Lijiang Observatory in 2011. *Solar Phys.* **293**(1), 1. DOI. ADS.

Authors and Affiliations

F.A. Iglesias[1] · C. Francile[2] · J. Lazarte-Gelmetti[2] · L.A. Balmaceda[3,4] · H. Cremades[1] · F. Cisterna[1]

✉ F.A. Iglesias
francisco.iglesias@um.edu.ar

C. Francile
cfrancile@unsj-cuim.edu.ar

J. Lazarte-Gelmetti
julilazarte95@gmail.com

L.A. Balmaceda
lbalmace@gmu.edu

H. Cremades
hebe.cremades@um.edu.ar

F. Cisterna
f.cisterna@alumno.um.edu.ar

[1] Grupo de Estudios en Heliofísica de Mendoza, CONICET, Universidad de Mendoza, Mendoza, Argentina

[2] Observatorio Astronómico Félix Aguilar, Universidad Nacional de San Juan, San Juan, Argentina

[3] George Mason University, Fairfax, VA 22030, USA

[4] NASA Goddard Space Flight Center, Heliophysics Science Division, Greenbelt, MD 20771, USA